공학석사 학위논문

Radiogenomic Analysis of Tumor Metabolism and Heterogeneity in Head and Neck Squamous Cell Carcinoma: Integration of FDG PET and Genomic Analysis

두경부 편평세포암종에서의 종양 대사 및 이질성에 대한 라디오지노믹스 분석: FDG PET 및 유전체의 통합적 분석

2019 년 12 월

서울대학교 융합과학기술대학원

융합과학부 방사선융합의생명전공

최 진 영

Abstract

Radiogenomic Analysis of Tumor Metabolism and Heterogeneity in Head and Neck Squamous Cell Carcinoma: Integration of FDG PET and Genomic Analysis

Jin Yeong Choi

Biomedical Radiation Sciences

Graduate School of Convergence Science & Technology

Seoul National University

The association of the metabolic and genomic heterogeneity features has not been well evaluated. This study was to evaluate the association of heterogeneity features of FDG PET with a tumor heterogeneity signature from genomic data and to explore the potential additive prognostic value of combining genomic heterogeneity

and metabolic imaging features in head and neck squamous cell carcinoma (HNSC).

Genomic, clinical and FDG PET data were obtained from the head and neck squamous cell carcinoma dataset in the cancer genome atlas (TCGA) and the cancer imaging archive (TCIA). The mutant-allele tumor heterogeneity (MATH) score (n = 508), the standard deviation of copy number variation (CNV std) (n = 492), and tumor glycolysis signature (GlycoS, n = 503) were gained from genomic data. Thirty-three patients were available for FDG PET images. Two tumor metabolic features (SUVmax, SUVpeak), two metabolic-volumetric (MTV, TLG) and two metabolic heterogeneity features [entropy, coefficient of variation (COV)] were obtained from the primary tumor.

Both genomic and FDG PET data were available in 25 patients. Among FDG PET features, MTV (P = .01), TLG (P = .02), entropy (P = .01) and COV (P = .04) showed significant correlation with MATH. We used GlycoS as a delegate for the metabolic imaging feature for survival analysis. 499 patients were available for both MATH and GlycoS. Also, lower MATH and GlycoS were associated with significantly better overall survival (n = 499, P = 0.002 and 0.0001 for MATH and GlycoS, respectively). Furthermore, both MATH and GlycoS independently predicted overall survival after adjusting for clinicopathologic features and the other (P = 0.015 and 0.006, respectively).

Tumor heterogeneity parameters assessed by FDG PET was

correlated with the tumor heterogeneity signature from genomic data in patients with HNSC. Glycolysis and heterogeneity signatures could further stratify the prognosis of the patients, which implies the potential of using both genomic and metabolic features for precise prognostication.

keywords : ^{18}F-fluorodeoxyglucose, positron emission tomography, heterogeneity, radiogenomics, MATH

Student Number : 2018-29025

Contents

List of Figures

List of Tables

Chapter 1. Introduction

1.1 Head and neck cancer

Head and neck cancer is a epithelial malignancies appearing in the oral, nasal cavity, larynx and pharynx. Head and neck cancer is the sixth common cancer in worldwide occupying approximately 6% of all malignancies breaking out over 550,000 new cases each year [1]. In 2017, about 50,000 new diagnoses and 10,000 deaths in united states. Also the incidence rate of head and neck cancer and mortality is about 3 times higher in males between 2009 and 2013. Five-year survival rates were 64% in oral cavity and pharynx cancers in all stages and races [2, 3].

Most of the head and neck cancer are head and neck squamous cell carcinoma (HNSC) and their main risk factors are abuse of tobacco and alcohol and infection of Human Papilloma Virus (HPV). Heavy smokers showed 5 to 25 fold higher risk of occurring HNSC than nonsmokers. Alcohol has also independent and multiplicative combined effect in 75% of all HNSC when consuming with cigarette. It is well known that chewing a betel quid is a risk factors of oral cavity cancer [4]. Recently the development of nasopharyngeal cancer is closely related to the infection of Ebstein Barr virus. In addition, HPV, type 16 and lesser extent type 18, has been found in about 15

to 50% of oropharyngeal squamous cell carcinoma. HPV related HNSC is more common in nonsmokers, nondrinkers. Oncogenic HPV types such as HPV16 and HPV 18 have a carcinogenic effect inactivating the tumor suppressor proteins like P53 and PRb through viral oncoproteins. HPV status is a crucial predictive biomarker and has implications for a treatment, and prognosis. HPV positive status showed a better prognostic factor and treatment response to radiation and chemotherapy because of susceptible tumor specific antigens [5, 6]. Cancer staging is a traditional prognostic biomarker in current. The size and infiltration of the tumor, lymph node metastasis and distant metastasis are used for deciding the stage [7].

Symptoms of HNSC is sore throat, lumps, mouth ulcer, bleeding and cough. Diagnosis and staging of HNSC are performed by laryngoscopy, oesophagoscopy, biopsy and imaging such as CT, MRI and PET-CT. Most metastasized site is lung, bones and liver. For the assessment of metastasis, chest imaging, bone scan, ultrasonography and esophagography. American Joint of Committee on Cancer staging is commonly used and classified the standard by the primary site. 18F-fluorodeoxyglucose positron emission tomography (FDG PET) comining with CT imaging is gradually used with the advantage of imaging precise lesions covering nodal and distant metastasis in whole body by one examination [7].

A standard of treatment of HNSC is a surgery, however, radiotherapy and chemotherapy is preferable in some cases for functional preservation of organs. Surgery gives an information about staging,

uninvolved micrometastasis, and treatment planning. Early stage tumor in a salivary gland, oral cavity, pharynx and larynx can be treated by surgical management. Radiotherapy is implemented for primary or adjuvant treatment. Tumor in larynx or pharynx can also be treated by radiotherapy because of a functional preservation. Radiotherapy is a primary therapy in early stage tongue and tonsillar cancer. A radiation dose of HNSC treatment is 2 Gy in a day for 5 days in a week to a total dose of 70 Gy. Altered fractionation methods such as hyperfractionation and accelerated fractionation with controlled radiation doses are in clinical trials for efficient treatment [7, 8]. Chemotherapy of HNSC uses platinum compounds, antimetabolites and taxanes. Cisplatin in a standard compound in chemoradiotherapy. Carboplatin and taxane based drugs are often used. Recently EGFR inhibition is arising a critical treatment of HNSC, so cetuximab and gefitinib are in clinical trials [9, 10].

1.2 Assessment of intra-tumor heterogeneity

Cancer is a heterogenous disease at genetic, epigenetic and phenotypic levels [11]. Genetic clonal evolution and cancer stem cell hypothesis are discussed as a cause of intratumor heterogeneity of cancer [12, 13]. Cancer stem cells which begins from a normal stem cell with self-renewal abilities raise tumor progression. After that, their differentiation makes tumor heterogeneous [14, 15]. Cancer progression is driven by a genetic process of clonal evolution, which eventually causes tumor genetic heterogeneity, a tumor with multiple subsets of subclonal mutations [11]. In clonal evolution model, mutations arise in a random normal cell with advantages of cell growth. Additional mutations make a tumor progression with genetic instability and advantages of cell survival [16]. Acquired tumor genetic heterogeneity is caused by the selective pressures during the evolution process and affected by tumor vasculature and an immune system in the microenvironment [17]. Furthermore, genetic heterogeneity eventually drives the phenotypic heterogeneity of a tumor by interacting environmental factors [18]. Heterogeneous subsets of a tumor have different molecular targets, which may result in different levels of resistance to the cancer treatment [19]. Accordingly, tumor heterogeneity is associated with the progression and eventual clinical outcomes of cancer patients [20]. Thus, evaluation of tumor heterogeneity is crucial for selecting anticancer strategies and predicting clinical outcomes [21].

Advances in next-generation sequencing (NGS) have allowed for extensive understanding of tumor genetic heterogeneity and provided useful features to evaluate of tumor heterogeneity [22, 23]. A bioinformatic method for allelic copy number, tumor purity and mutation variant allele frequency is used as an assessment of clonal evolution of somatic mutation [17]. A multiregional biopsy from the same tumor is efficient to analyze tumor evolution from spatial mutations and phylogenetic relationships [17, 24]. In a study of multiregion sequencing for intratumor heterogeneity, they performed whole exome sequencing and RNA sequencing about nine primary tumor regions and additional metastatic regions from renal cell carcinoma patients. They analyzed the somatic mutations and phylogenetic trees and ploidy profiling from each of regions [24]. Single cell sequencing is also useful for revealing intratumor heterogeneity. It gives more comprehensive information about evolutionary process from each cancer cells in genetic, transcriptomic and epigenetic level [25]. The mutant allele tumor heterogeneity (MATH), a genetic heterogeneity feature, is easily calculated as a percentage of mutant allele frequencies among tumor-specific mutated loci including all genes. MATH has been known to have a prognostic value in HNSC and colon cancer [26, 27]. Also, to compare the MATH with the other genetic heterogeneity signature, we used the standard of deviation of copy number variation (CNV std). Copy number variation is structural variation of the genome by deletions and duplications of a specific region of DNA. This region includes

~50 base pairs to mega base pairs [28]. The difference in DNA copies associated cancer progression and development [29, 30]. In previous study, they showed copy number variation is more robust predictor than allele frequency variation by comparing MATH and CNV std because of the change of MATH according to mutation callers [31]. However, CNV std is not a representative feature of intra-tumor genetic heterogeneity, and its potential as a prognostic biomarker has not been validated.

Hematoxylin and Eosin (H&E) staining and flow cytometry is conventional methods for cell phenotype analysis using tumor specimens. Flow cytometry is a quantitative multicolor fluorescence measuring system in cell levels. In the past, flow cytometric method is used for phenotypic intratumor heterogeneity using quantitation of DNA, tumor markers and cellular antigen molecules with different dyes [32]. Nowadays, this method is used as a tool of isolating a single cells for a single cell sequencing studies [33, 34]. Pathologists can guess a quantity of lymphocytes and cancer cell nucleus, molecular subtype, growth rate and drug resistance with H&E staining [35, 36]. These histopathological characters correlated with genetic and transcriptomic heterogeneity [36, 37]. Phenotypical heterogeneity can also be noninvasively studied using various imaging techniques including computed tomography (CT), magnetic resonance imaging (MRI) and 18F-fluorodeoxyglucose positron emission tomography (FDG PET) [38]. FDG PET is a compelling image modality to evaluate metabolic heterogeneity of tumors, a phenotypic

tumor heterogeneity [39]. Recently, heterogeneity parameters obtained using FDG PET have been extensively evaluated and reported to have diagnostic and prognostic values in multiple types of malignancies including HNSC, non-small cell lung cancer, and pancreatic cancer [39-43]. Although the metabolic features evaluated by FDG PET are closely associated with biological factors in the tumor microenvironment [39, 44, 45], it is still unknown whether metabolic heterogeneity is associated with genetic heterogeneity [41].

1.3 FDG PET for measurement of tumor metabolism and heterogeneity

In FDG, hydroxyl group at C-2 position of glucose is placed by ^{18}F. FDG, a glucose analogue, is more consumed in tumor cells with high rates of glycolysis. When FDG enters into the tumor cell by glucose transporter protein without ATP, it becomes FDG-6-phosphate by hexokinase. FDG-6-phosphate dose not metabolite for further glycolysis pathway because of the substitution of oxygen atom in C-2 position. Since polar phosphorylated FDG cannot pass through the cell membrane, FDG-6-phosphate is trapped inside the cell. Because FDG-6-phosphate to FDG reverse reaction mediated by glucose-6-phosphate only happens in liver, intestine and renal cells. Therefore, FDG is completely trapped and high intake of FDG is mainly observed in brain, heart and tumor cells. Cells with high concentration of FDG reflects metabolically active cells with increased activity of glucose transporter and hexokinase [46, 47].

^{18}F-2-deoxy-2-fluoro-D-glucose positron emission tomography (FDG PET) is non-invasive and helpful in staging of the cancer and predicting prognosis and treatment outcome with understanding of tumor metabolism [48]. FDG PET is used for staging of lung cancer, malignant melanoma, colorectal cancer, lymphomas, head and neck cancer, gastroesophageal cancer, breast cancer and thyroid cancer [49, 50]. FDG PET imaging has the limitations that there is no accurate

measurement standard to evaluate treatment response, but it has the advantage of cost effectiveness and easy modality to assess cancer staging, recurrence, metastasis and treatment outcome in whole body [49]. In head and neck cancer, primary tumor staging and lymph node staging with FDG PET are more accurate than conventional imaging [51-53]. Changes of anatomic structures after radiation therapy and surgery make a difficult to use MR and CT for assessment of residual region and recurrence. FDG PET showed better sensitivity than other modalities in estimating response to treatment and recurrence [54-56]. Despite the advantage of higher sensitivity, FDG PET has the limitation of false positive results due to infection and inflammation after surgery and treatment [51, 57].

FDG PET imaging gives not only a qualitative information but also a quantitative information about the radioactivity concentrations of FDG. For example, standardized uptake value (SUV) provide the radioactivity at the time point of imaging. SUV is calculated by normalizing a voxel intensity to the injected dose and body weight [46]. Maximum standardized uptake value (SUVmax) is a value for one voxel having the highest intensity among the region of interest (ROI). Peak standardized uptake value (SUVpeak) is an average of voxel intensities located at a defined size ROI. SUVpeak is a more robust parameter than SUVmax in a heterogeneous tumor because SUVmax represent only one voxel in tumor. However, SUVpeak is also has a limitation about the unclear standard of drawing ROIs. Volumetric parameters such as metabolic tumor volume (MTV) and

total lesion glycolysis (TLG) are derived the volume of FDG activity in ROI for measuring tumor glycolysis. MTV is a volume of the ROI and TLG is calculated by multiplying SUV and MTV. Conventional FDG parameters are reported to have a prognostic value in cancer patients [58-60].

Recently, various methods analyzing the tumor heterogeneity using texture analysis are studied. Histogram, absolute gradient, run-length matrix, and co-occurrence matrix are commonly used method for tumor heterogeneity texture parameters [61-63]. Grey-level values are a brightness of a pixel. Lower values represent darker levels. The maximum grey level is relevant with bits of the image. Histograms display a number of pixels at each grey level values. Histogram based features are mean, variance and percentiles from this histogram. Gradient is an extent of the variation of grey level values. Absolute gradient parameters are also a mean and variance of gradient. Run-length matrix represents the distance from the grey level of a point pixel to the same grey level value in a particular direction. The co-occurrence matrix indicates how much a pair of intensity located in a specific direction and distance exists in the ROI. Heterogeneity parameters such as entropy, contrast and homogeneity is computed with this method [61-65].

1.4 Research objectives

Herein, we investigated if metabolic heterogeneity based on FDG PET was associated with genetic heterogeneity represented by MATH and CNV std. Furthermore, we explored the prognostic value of both metabolic and genetic heterogeneity features in predicting the outcomes of cancer patients.

Chapter 2. Materials and methods

2.1 Data acquisition

Genomic and clinical data were obtained from the head and neck squamous cell carcinoma dataset of the cancer genome atlas (TCGA-HNSC). The FDG PET data of the patients included in TCGA-HNSC was obtained from cancer imaging archive (TCIA) which are a publicly available repository. TCGA and TCIA data were acquired by a publicly available dataset that removed patient identifiers. The publicly available data were collected with patients' informed consent approved by the institutional review boards of all participating institutions following the 1964 Helsinki declaration and its later amendments or comparable ethical standards. Total 528 clinical information which was updated at 2018/08/30 were acquired National Cancer Institute database for the survival analysis. The somatic variants data were acquired for 508 TCGA-HNSC patients from the NCI database using R data package 'TCGAmutations'. Copy number variation data was download from 'TCGAbiolinks' R package. We selected data type as masked copy number segment for the removal of germline mutations. Glycolysis signature (GlycoS) was previously assessed for the metabolic signatures of all TCGA samples [66] and downloaded from the website

(http://choih.shinyapps.io/metabolicsignatures). In brief, GlycoS data were obtained by RNA sequencing data of TCGA samples by using gene set enrichment analysis and metabolic pathway genes of Reactome [67]. Total 192 patients of TCGA-HNSC images in the TCIA matched with the genomic data of the TCGA were available. Finally, we identified 33 cases which included baseline FDG PET/ computed tomography (CT) scans and utilized the FDG PET scans for further analysis.

2.2 Tumor metabolic features analyzed by FDG PET

In this study, primary tumor segmentation of all FDG PET examinations was computed using PETedge tool of MIMvista (MIM Software Inc., USA) by an expert. Before calculating the texture feature, we have changed X, Y, Z values of all data sets as the same values (4.7, 4.7, 3.3) through trilinear voxel interpolation to compare each other. Then feature extraction was performed using LIFEx (IMIV, CEA, France) based on these regions of interest (ROIs)[68]. SUVmax, SUVpeak, MTV and TLG are the conventional metabolic or metabolic-volumetric parameters which are the most extensively studied in the previous studies and found to be prognostic in head and neck cancer [69-71]. Among the many heterogeneity parameters, we selected entropy and COV because these features were reproducible and robust values in different reconstruction and acquisition time settings according to previous studies [72, 73]. Two tumor metabolic features [maximum standardized uptake value (SUVmax), peak standardized uptake value (SUVpeak)], two metabolic-volumetric [total lesion glycolysis (TLG), metabolic tumor volume (MTV)] and two metabolic heterogeneity features [entropy, and coefficient of variation (COV)] were obtained. Entropy was calculated based on SUV histogram using the equation; $-\sum_i p(i) \times \log_2(p(i) + \varepsilon)$. Entropy reflects the randomness of the

distribution where p(i) is the probability of occurrence of voxels with intensity i and ε = 2e-16. COV was calculated as standard deviation divided by SUVmean of the ROI. There were small tumors among the patients (range 0.36 ~ 3.93 mL, median 1.14 mL). However, we could calculate entropy and COV in all tumors, because Entropy was the histogram-based parameter and COV can be calculated from SUV distribution. Twenty-five head and neck squamous cell carcinoma (HNSC) cases which have both FDG PET feature extraction data and gene mutation data were available to perform correlation analysis.

2.3 Tumor genetic heterogeneity

The MATH score was obtained as a percentage of the median absolute deviation (MAD) and median by clustering the variant allele frequency in each mutated loci using the R 'maftools' package [74]. Each MATH score was calculated using MAF files for a total of 508 tumor samples, and this was used for survival analysis together with survival data.

The CNV std is a value of standard deviation of 'segment Mean' column from the 'nocnv' files in each patients. Same as a previous study [75], we also set a threshold of 0.2 of amplification and -0.2 of deletion in segment mean values for using high confidence CNV values.

2.4 Survival analysis

Overall survival (OS) can be obtained from the clinical data, which is defined as the period from the date of diagnosis until the date of death from any cause. The censored time is from date of initial diagnosis until the date of last contact (largest number of days) from all the clinical data files [76]. For evaluation of prognostic value of the features, we divided the patients into two groups (high and low groups) according to an optimized cut-off of each feature. The optimized cut-off was selected using the 'cutoff finder (http://molpath.charite.de/cutoff/index.jsp)'. We selected the method for 'Survival: significance (log-rank test)' for cutoff determination. This cutoff is the most significant point from log-rank test which divide the variables into two groups. The high and low groups were compared using the log-rank test and Kaplan Meyer analysis. Cox regression analysis was also performed in multivariable survival analysis using continuous MATH, continuous CNV std, GlycoS, age and categorical clinicopathologic variables (sex and tumor stage).

2.5 Statistical analysis

Association between these genomic and tumor metabolic features was analyzed by using correlation analysis and the prognostic value of the parameters were assessed using the log-rank test. To analyze the correlation between two genomic and selected six FDG PET features, Spearman correlation analysis was performed. Correlation analysis except FDG PET features was done by Pearson correlation method. Correlation coefficients and p-values were gained and used to sort statistically significant features (p-value $<$ 0.05). All statistical analyses were performed in R (version 3.4.4) and SPSS (version 25). All tests were two-sided and p-values less than 0.05 were considered significant.

Chapter 3. Results

3.1 Patients characteristics

The scheme of this study is demonstrated in **Figure 3.1.** The number of patients with genomic data was 508. The patients had a median age of 61 years (range of 20-90 years) and a median follow-up days of 633 days (range of 2-6417 days). Among them, 220 patients died during the follow-up. In all patients, seventy-eight percent were stage III/IV, and there were an about three times higher number of men than women (371 vs. 137).

The characteristics of twenty-five patients who were available for both genomic and FDG PET analysis are summarized in **Table 3.1.** Primary tumor segmentation and feature extraction were performed using FDG PET scans of the patients. The median age of the patients was 56 years (range of 38-84 years). Among twenty-five patients with a median follow-up of 458 days (range of 30-6417 days), six patients died while eighteen were alive.

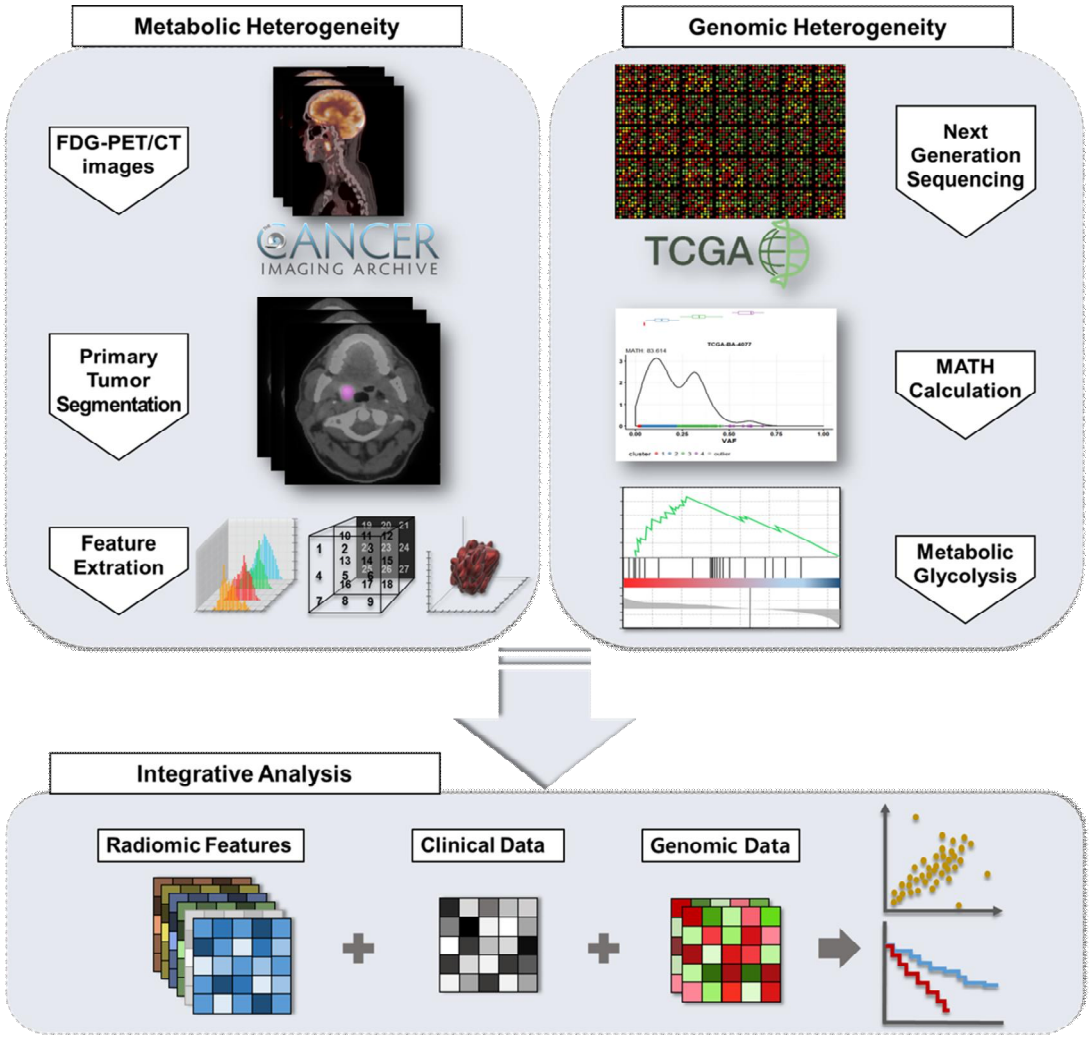

Figure 3.1 Study scheme

A scheme for integrative study of radiogenomics. FDG PET data and genomic mutation data for TCGA-HNSC dataset were obtained from each database of TCIA and TCGA. (A) The primary tumor was manually assigned, and then ROIs were computed for feature extraction. (B) MATH calculation using MAF files were done in R. Also, metabolic glycolysis (GlycoS) value was obtained using gene set enrichment analysis. (C) Clinical data of TCGA-HNSC was gained from TCGA. Total six features were selected and used for

radiogenomic analysis. We statistically analyzed radiomic, clinical and genomic data using correlation analysis, Kaplan-Meier analysis, log-rank test.

Patients, n	25 (1 of not available clinical data)
Median follow-up (days)	458 (30-6417)
Vital status Dead Alive	 6 18
Age (years) Median Range	 56 38 ~ 84
Gender Male Female	 18 6
Clinical stage I II III IVA IVB IVC	 3 5 2 13 1 0
Tumor site Alveolar Ridge Base of tongue Larynx Oral cavity Oral tongue Tonsil	 1 2 5 4 3 9

Table 1. Patients characteristics (FDG-PET)

3.2 Association between genetic and FDG PET features

Correlation analyses between MATH, CNV std, GlycoS and FDG PET features (SUVmax, SUVpeak, TLG, MTV, entropy, and COV) were performed in 25 patients.

MATH and CNV std representing of genetic heterogeneity was associated (ρ = 0.560, P = 0.001)(**Figure 3.2**). Metabolic heterogeneity features and metabolic-volumetric features showed a trend for association with the genetic heterogeneity feature, MATH (ρ = 0.488, P = 0.013 for entropy; ρ = 0.402, P = 0.047 for COV, ρ = 0.521, P = 0.008 for MTV; ρ = 0.472, P = 0.017 for TLG) with statistical significance (**Figure. 3.3 and 3.4**). On the other hand, SUVmax and SUVpeak were not significantly associated with MATH (ρ = 0.328, P = 0.110 for SUVmax; ρ = 0.286, P = 0.250 for SUVpeak) (**Figure 3.3**). CNV std was not associated with metabolic and metabolic heterogeneity features (ρ = 0.118, P = 0.575 for SUVmax; ρ = 0.189, P = 0.453 for SUVpeak; ρ = 0.272, P = 0.188 for entropy; ρ = 0.322, P = 0.117 for COV). But, metabolic volumetric features showed a tendency of positive correalation. (ρ = 0.408, P = 0.043 for MTV; ρ = 0.369, P = 0.069 for TLG) (**Figure 3.5**).

We evaluated the association between GlycoS calculated by gene expression and FDG PET features to use GlycoS as a surrogate of tumor metabolic features for more patients in survival analysis. TLG

and MTV from FDG PET showed moderate degree of associations with the GlycoS (ρ = 0.590, P = 0.002 for MTV; ρ = 0.570, P = 0.004 for TLG). The GlycoS showed a trend of positive correlation with entropy, while COV, SUVmax and SUVpeak did not (ρ = 0.519, P = 0.009 for entropy; ρ = 0.393, P = 0.057 for COV; ρ = 0.331, P = 0.114 for SUVmax; ρ = 0.272, P = 0.291 for SUVpeak) (**Figure 3.6**).

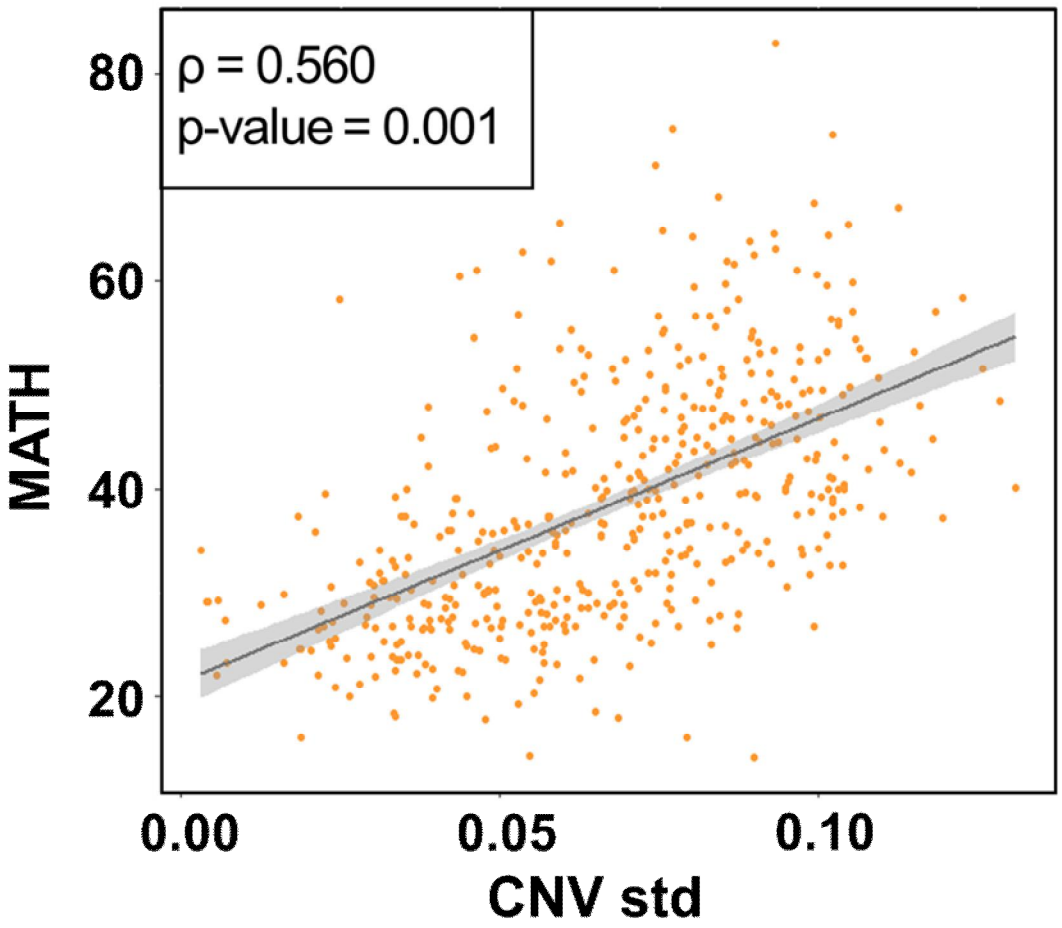

Figure 3.2 Correlation between MATH and CNV std

Scatter plots for correlation analysis of MATH and CNV std. Each orange dots represent patients available for MATH and CNV std (N=492). Upper left box shows Pearson correlation coefficient (ρ) and p-value. The dark gray line means a linear regression line and the gray region is 95% confidence region.

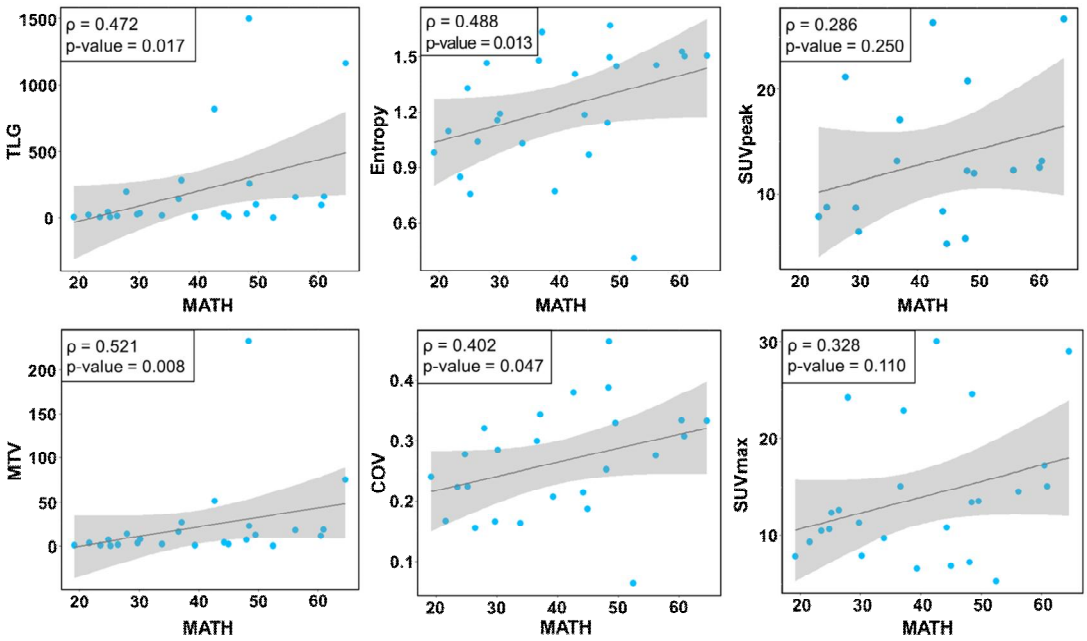

Figure 3.3 Correlation between MATH and FDG PET features

Scatter plots for correlation analysis of MATH and FDG PET features. Each blue dots represent patients available for MATH and radiomic data (N=25). Upper left box shows Spearman correlation coefficient (ρ) and p-value. The dark gray line means a linear regression line and the gray region is 95% confidence region.

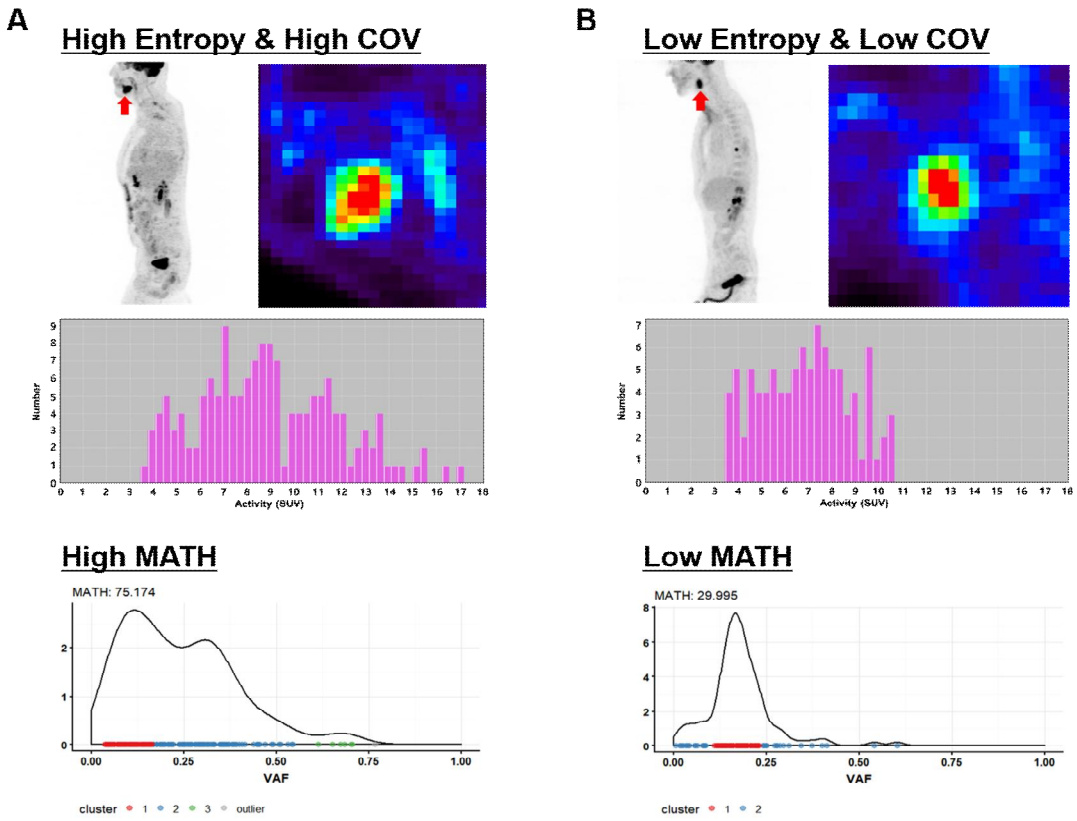

Figure 3.4 Representative cases

(A) A patient had a tongue cancer with high metabolic heterogeneity (high entropy and high COV groups). Genomic analysis of the patient revealed that the tumor had high genetic heterogeneity (high MATH group). (B) A patient had a left tonsillar cancer with low metabolic heterogeneity (low entropy and low COV group) based on FDG PET. Genomic analysis of the patient revealed that the tumor had low genetic heterogeneity (low MATH group).

Of note, low and high entropy, COV, and MATH groups are divided according to the optimized cut-offs obtained by cut-off finder (http://molpath.charite.de/cutoff/index.jsp).

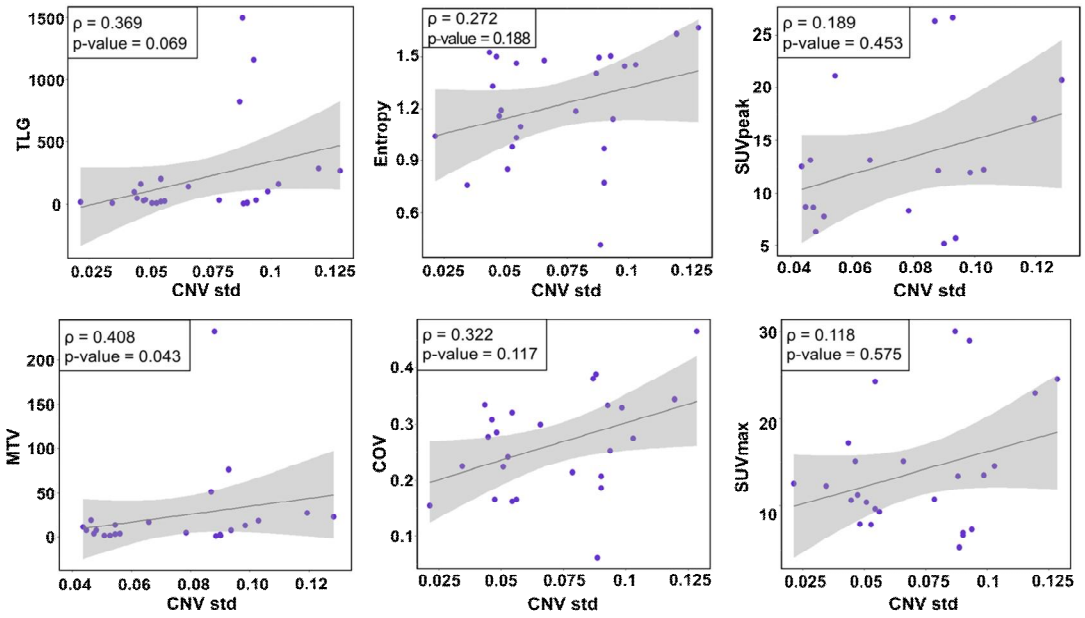

Figure 3.5 Correlation between CNV std and FDG PET features

Scatter plots for correlation analysis of CNV std and FDG PET features. Each purple dots represent patients available for CNV std and radiomic data (N=25). Upper left box shows Spearman correlation coefficient (ρ) and p-value. The dark gray line means a linear regression line and the gray region is 95% confidence region.

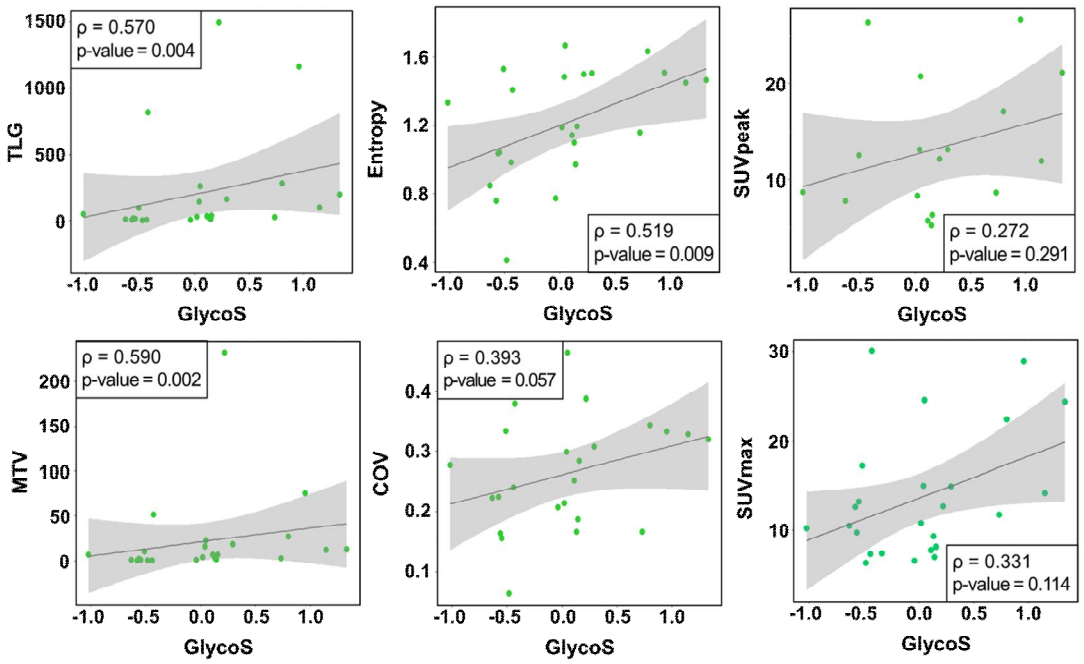

Figure 3.6 Correlation between GlycoS and FDG PET features

Scatter plots for correlation analysis of GlycoS and FDG PET features. Each green dots represent patients available for GlycoS and radiomic data (N=25). Upper left box shows Spearman correlation coefficient (ρ) and p-value. The dark gray line means a linear regression line and the gray region is 95% confidence region.

3.3 Prognostic value of the genetic and FDG PET features

We analyzed the prognostic value of genetic and FDG PET features. SUVmax, MTV, TLG, and entropy were predictive of OS ($P < 0.05$ for the features), while COV tended to predict the OS ($P = 0.072$) (**Figure. 3.7**).

Also, MATH and CNV std tended to predict the OS ($P = 0.086$ for MATH and $P = 0.059$ for CNV std) in the 25 patients. Thus, we tested the predictive value of using both heterogeneity features from genetic data and FDG PET. We divided the patients into two groups (low and high) based on both metabolic and genetic heterogeneity features. Low group consists of patients who are in low group for both MATH/CNV std and FDG PET feature (COV or entropy) and high group consists of patients who are in high group for MATH/CNV std and/or FDG PET feature (COV or entropy). We found that the combination of MATH and FDG heterogeneity features showed more robust predictive value of OS than using only MATH (MATH: $P = 0.086$, MATH+COV: $P = 0.024$, MATH+Entropy: $P = 0.012$, **Figure. 3.8**). On the other hand, CNV std and FDG heterogeneity did not showed any prognostic values (CNV std: $P = 0.059$, CNV std+COV: $P = 0.086$, CNV std+Entropy: $P = 0.055$, **Figure. 3.9**).

Finally, we further analyzed the prognostic value of MATH/CNV std

and GlycoS in about 500 patients. We found that MATH, CNV std and GlycoS were highly predictive of OS in univariate analysis using log-rank test and Kaplan Meyer analysis (P = 0.002 for MATH; P = 0.013 for CNV std; P = 0.0001 for GlycoS) (**Figure. 3.10**). MATH and GlycoS were predictive of OS even after adjustment using clinicopathologic features (age, sex, and tumor stage) in multivariate Cox regression analysis. Furthermore, both MATH and GlycoS were still significant prognostic factors even after including both features and the clinicopathologic features in the same model. This result indicates that both features have an additive role over each other to predict OS (P = 0.015 for MATH; P = 0.006 for GlycoS) (**Table 3.2**). However, CNV std was prdictive of OS in univariate analysis and not predictive in multivariate analysis after adjusted by clinicopathologic features and GlycoS (P = 0.035 in univariate analysis; P = 0.106 after adjusted)(**Table 3.3**)

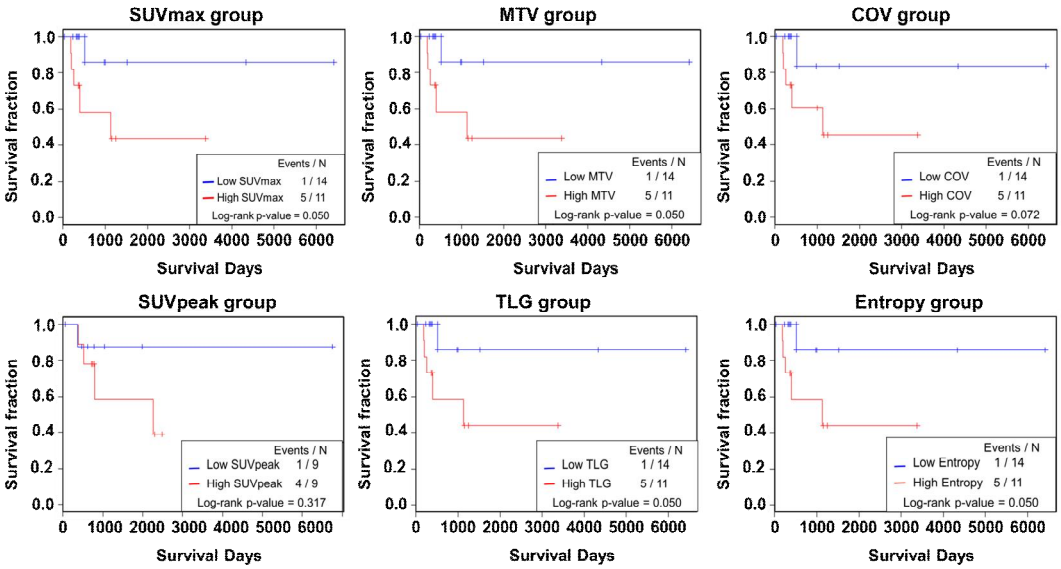

Figure 3.7 Prognostic value of FDG PET features

Kaplan-Meier curves of each group divided with adjusted cutoff value of FDG features. Survival analysis and log-rank test were performed to compare each group. Low and high FDG subsets for 25 patients. Red, high subset; blue, low subset.

Of note, low and high FDG features are divided according to the optimized cut-offs obtained by cut-off finder (http://molpath.charite.de/cutoff/index.jsp).

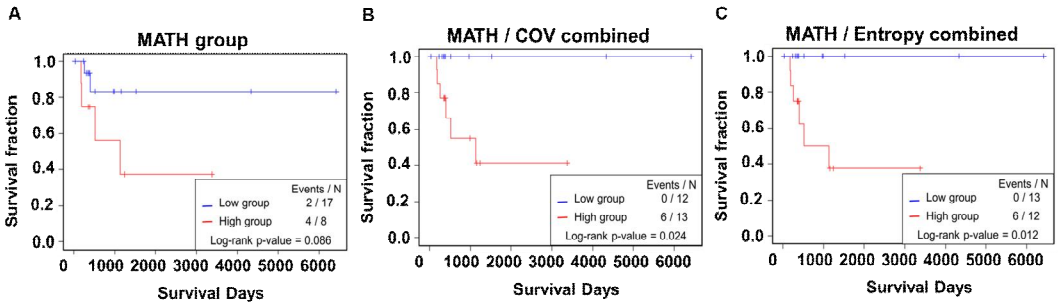

Figure 3.8 Predictive value of combined MATH and FDG PET features

Kaplan-Meier curves of each group divided with adjusted cutoff value of the features. **(A)** MATH showed a trend of prediction of OS (P = 0.086). **(B, C)** When MATH and FDG features were combined, the predictive value became more robust (B: MATH+COV, P = 0.024, C: MATH+Entropy, P = 0.012). Low group = patients in low group for both features; High group = patients in high group at least one feature.

Of note, low and high groups are divided according to the optimized cut-offs obtained by cut-off finder (http://molpath.charite.de/cutoff/index.jsp).

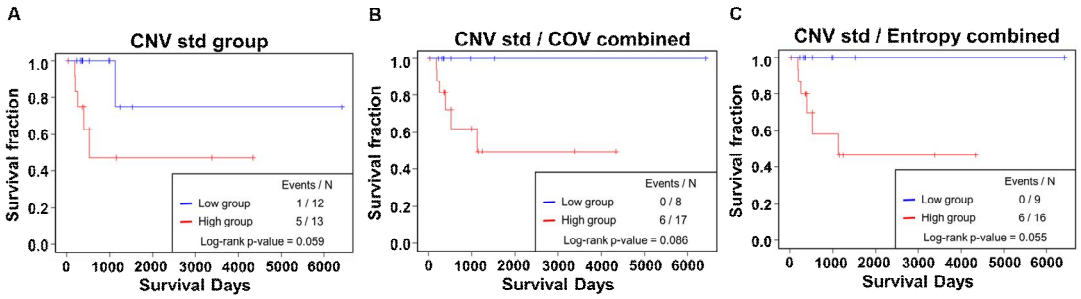

Figure 3.9 Predictive value of combined CNV std and FDG PET features

Kaplan-Meier curves of each group divided with adjusted cutoff value of the features. **(A)** CNV std showed a trend of prediction of OS (P = 0.059). **(B, C)** CNV std combined with metabolic heterogeneity features showed a trend of prediction of OS. (B: CNV std+COV, P = 0.086, C: CNV std+Entropy, P = 0.055). Low group = patients in low group for both features; High group = patients in high group at least one feature.

Of note, low and high groups are divided according to the optimized cut-offs obtained by cut-off finder (http://molpath.charite.de/cutoff/index.jsp).

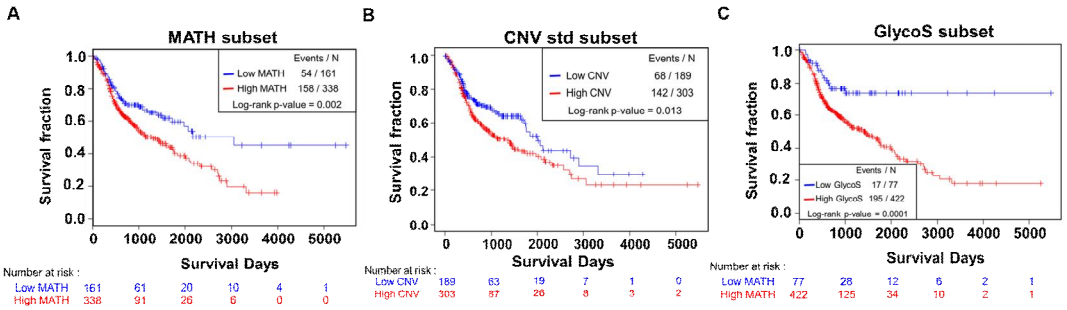

Figure 3.10 Prognostic value of MATH, CNV std and GlycoS

Kaplan-Meier curves of each group divided with adjusted cutoff value of genetic signatures. Survival analysis and log-rank test were performed to compare each group. (**A**) Low MATH and high MATH subsets for 499 patients. Red, high MATH (MATH > 37.17); blue, low MATH (MATH < 37.17). (B) Low CNV std and high CNV std subsets for 492 patients. Red, high CNV std (CNV std > 0.05891); blue, low CNV std (CNV std < 0.05891). (C) Same analysis as (A) comparing low GlycoS and high GlycoS subsets. Red, high GlycoS (GlycoS > 0.80); blue, low GlycoS (GlycoS < 0.80).

Of note, low and high groups are divided according to the optimized cut-offs obtained by cut-off finder (http://molpath.charite.de/cutoff/index.jsp).

	Hazard ratio (95% CI)	P value
MATH (unadjusted)	1.013 (1.002-1.024)	0.016
MATH (adjusted for age, gender, and tumor stage)	1.016 (1.004-1.027)	0.007
MATH (adjusted for GlycoS, age, gender, and tumor stage)	1.014 (1.003-1.026)	0.015
GlycoS (unadjusted)	1.381 (1.129-1.689)	0.002
GlycoS (adjusted for age, gender, and tumor stage)	1.362 (1.112-1.668)	0.003
GlycoS (adjusted for MATH, age, gender, and tumor stage)	1.331 (1.085-1.633)	0.006

Table 3.2 Multivariate cox regression test for MATH and GlycoS

	Hazard ratio (95% CI)	P value
CNV std (unadjusted)	56.637 (0.313-10250.965)	0.128
CNV std (adjusted for age, gender, and tumor stage)	35.890 (0.183-7038.055)	0.184
CNV std (adjusted for GlycoS, age, gender, and tumor stage)	15.169 (0.078-2934.893)	0.311
GlycoS (unadjusted)	1.381 (1.129-1.689)	0.002
GlycoS (adjusted for age, gender, and tumor stage)	1.362 (1.112-1.668)	0.003
GlycoS (adjusted for CNV std, age, gender, and tumor stage)	1.347 (1.095-1.656)	0.005

Table 3.3 Multivariate cox regression test for CNV std and GlycoS

Chapter 4. Discussion

4.1 Summary

We found that the tumor metabolic features estimated by FDG PET showed a mild but statistically significant level of association with tumor genetic heterogeneity. Specifically, tumor metabolic-volumetric and metabolic heterogeneity features of FDG PET were associated with MATH in a mild degree. This finding supports the notion that quantifiable FDG uptake features reflect the tumor heterogeneity at the genomic level in HNSC [27]. Also, there was additive prognostic value when the FDG PET and genetic heterogeneity features were combined. Additionally, both genetic heterogeneity feature (MATH) and glycolysis feature (GlycoS) were independently predictive of OS even after adjusting for clinicopathologic features [77].

Meanwhile CNV std was associated with MATH values, involving CNV std and MATH can influence each other. But CNV std did not associated with metabolic heterogeneity features. CNV std was prognostic in HNSC, but when comibined with the metabolic features and its surrogate GlycoS in survival analysis, it did not showed improved prognositc value.

4.2 Association between genetic and FDG PET features

Recently, tumor imaging phenotypes were found to be related to gene expression profiles in HNSC [27, 44, 78-81]. Specifically, SUV and heterogeneity features estimated by FDG PET were related to 1177 differentially expressed genes in normal and tumor tissues [27]. Previous studies have shown a link between FDG uptake and several specific genes which modulate glucose metabolism [82-84]. Also, phenotypic whole tumor-level heterogeneity can be noninvasively recognized by various imaging techniques including computed tomography (CT), magnetic resonance imaging (MRI) and FDG PET [38]. However, it has been unclear whether the genetic heterogeneity assessed by a small sample of tumor tissue can reflect the whole tumor-level phenotypic heterogeneity or not [21]. Also, there has been no study to evaluate the association tumor heterogeneity measured by FDG PET and genomic analysis in patients with HNSC. As cancer cells are evolved in a heterogeneous spatiotemporal environment based on genetic heterogeneity, we hypothesized that genetic heterogeneity might be associated with whole-tumor level heterogeneity measured by FDG PET. In this study, by utilizing the database of TCGA and TCIA, we were able to find that there is an association between whole tumor level heterogeneity based on FDG PET and genetic heterogeneity in HNSC. Although the association

was statistically significant, the level of association was weak with correlation coefficients of 0.4 ~ 0.5. This weak level of association was not surprise because the methods to measure the tumor heterogeneity were totally different between FDG PET heterogeneity parameters and MATH. MATH was obtained from genetic sequencing data of a small portion of tumor, while FDG PET heterogeneity parameters were calculated from an imaging data reflecting metabolic status of a whole tumor area. It is noteworthy that there was a mild degree of association between MATH and FDG PET heterogeneity parameters, even with this striking difference of the methods to measure the tumor heterogeneity.

4.3 Genetic heterogeneity signatures

MATH is a genetic heterogeneity measure, which can be easily quantified as a percentage of mutant allele frequency among tumor-specific mutated loci. Also, the prognostic value of MATH has been validated in HNSC and colon cancer [26, 85, 86]. In the patients with HNSC, high MATH score was associated with increased mortality [85, 86]. Also, MATH was associated with the risk of metastases in patients with colon cancer [26]. However, the ability of MATH to represent tumor heterogeneity has not been tested by other modalities. We have demonstrated that MATH was highly associated with the representative heterogeneity features from FDG PET (entropy, COV). This result is in line with a recent study by Moon et al. They showed that Shannon's heterogeneity index was associated with entropy in patients with small cell lung cancer [87]. Furthermore, we found that MATH was predictive of OS in patients with HNSC even after adjusting clinicopathologic features.

Copy number variation is deletion and duplication of chromosomal segments. Copy number variations and MATH were positively correlated and stronger association was detected with allele frequency standard deviation for all tumor types in TCGA. In conclusion, they argued copy number variations can affect allele frequencies and thus get involved allele frequency distribution [31]. However, CNV data (segment number and mean square values) did not produced improved results in HNSC. CNV was not related to clinical variables like TP53

mutation, HPV status and pack years as opposed to MATH [88]. Our result also showed CNV std did not showed association with metabolic heterogeneity features and poorer prognostication than MATH. It is because MAF value distribution of mutated loci is affected by both subclonal mutations and copy number abberations (CNAs) [85]. In other words, intra-tumor heterogeneity calculated as MATH can be occurred by both CNAs and subclonal mutations.

4.4 FDG PET features

Recent meta-analyses showed that various FDG PET features including SUVmax, MTV and TLG were prognostic factors in multiple types of malignancies [28, 89-91]. Also, heterogeneity features of FDG PET have shown to be associated with treatment response and clinical outcome in multiple types of malignancies [40, 42, 92-94]. Among the heterogeneity features, entropy and COV have been widely accepted and proven to be useful for predicting treatment response and clinical outcomes [40, 42, 93]. For example, entropy was predictive of OS in pancreatic cancer [42], and the changes in entropy was independently associated with treatment response in erlotinib-treated non-small cell lung cancer [40]. Also, COV was superior to conventional parameters in predicting therapy response and disease progression in rectal cancer [93]. We found that entropy and COV were strongly associated with MATH, a genetic heterogeneity feature, which re-enforced the genetic background of the features and thus increased possibility of clinical utilization of the features.

MTV and TLG are radiomic features that represent metabolic-volumetric tumor burden. MTV is a measurement of tumor volume with increased glucose metabolism, while TLG is the product of MTV and the mean SUV of the volume. MTV and TLG are considered to be better prognostic factors than simple metabolic feature such as SUVmax [90, 95, 96]. In this study, we also found

that MTV and TLG are significantly associated with genetic heterogeneity. As the tumor spatially grows, the larger volume of tumor likely to be more heterogenous reflecting genetic heterogeneity by cancer evolution. Multiple studies have shown that MTV and heterogeneity features of FDG PET such as COV and texture features are associated [64, 97, 98]. Therefore, tumor metabolic-volumetric features are likely to be an indicator of tumor genetic heterogeneity due to cancer evolution. Also, the association of MTV and TLG with genetic heterogeneity may further explain the robustness of the features in predicting the clinical outcomes.

4.5 Glycolysis

Glycolysis is a crucial pathway regulating oncogenes, tumor suppressor genes, and glycolytic enzymes as well as accelerating cell proliferation in cellular metabolism [99]. Factors of metabolic glycolysis are associated with poor prognosis and tumor resistance to therapy in HNSC [100]. Also, glycolysis gene expression correlates FDG uptake features [79, 82-84]. However, the previous studies only explored the relationship of representative genes such as glucose transporter (GLUT) or hexokinase (HK). On the other hand, we utilized a novel glycolysis signature, GlycoS, which was derived from multiple glycolysis associated genes defined by Reactome [66, 101]. We found that metabolic-volumetric features (MTV, TLG) were significantly associated with GlycoS. Unexpectedly, SUVmax, and SUVpeak were not associated with GlycoS. One potential explanation is that many glycolysis associated genes may not influence the intensity of FDG uptake, because the FDG uptake kinetics are primarily determined by glucose transportation by GLUT and phosphorylation by HK [102]. Even though, a higher number of patients may prove the associations between SUVmax and GlycoS, since there was a trend of positive correlation ($P = 0.114$). Also, we found that GlycoS is predictive of OS in patients with HNSC. Furthermore, GlycoS was predictive of OS even after adjusting MATH and clinicopathologic features. This implies that GlycoS has an additive prognostic value over MATH.

4.6 Limitation of study

There are several limitations to this study. First, a limited number of samples were available in public archives. Also, we found only a mild degree of association between the genetic and FDG PET heterogeneity, and there were large number of scatters outside of the standard deviation (**Figure 3.3**). Further studies will yield clearer results if analyzed using a larger number of expanded data. Second, FDG PET data from TCIA were applied to different technologies, reconstruction, and attenuation correction methods. So each image is difficult to compare to each other, and even SUVmax values vary, which may affect clinical decision [103]. To solve this problem, we did voxel interpolation to make all images have uniform voxel sizes. Also, we used entropy and COV as a tumor heterogeneity texture features because these are the most reliable upon reconstruction method. Third, although metabolic features and genomic signatures obtained this study were candidates for future biomarkers, these are not validated precisely. Although we used representative genomic and metabolic features which have clinical implications with prognosis, there might be better features than these eight features. Fourth, since the analysis of intratumor heterogeneity using MATH or CNV using TCGA data does not include consideration of whole regions within the same tumor, it should be analyzed with genetic data using multiregional sequencing or single cell sequencing. In a future study,

more features could be considered for understanding cause and effect through systemic tumor biology. Nonetheless, our results show a correlation between genetic heterogeneity features and metabolic heterogeneity features and prognostic value about each feature.

Chapter 5. Conclusion

CNV std had a prognostic value in head and neck cancer but not appeared advantages in prognosis and correlations with metabolic features. MATH, as a tumor genetic heterogeneity presenting both subclonal mutations and CNVs was associated in a mild degree with metabolic heterogeneity measured by FDG PET in patients with HNSC. Genetic and metabolic heterogeneity features were predictive of OS and there was additive prognostic value when the FDG PET and MATH were combined. Moreover, genetic heterogeneity feature (MATH) and glycolysis feature (GlycoS) were independent predictors of OS for precise prognostication.

References

[1] E. Du et al., "Long-term Survival in Head and Neck Cancer: Impact of Site, Stage, Smoking, and Human Papillomavirus Status," 2019.

[2] S. Rebecca, M. Siegel, D. Kimberly, M. Miller, and D. J. C. C. J. C. Ahmedin Jemal, "Cancer statistics," vol. 67, no. 27, pp. 7-30, 2017.

[3] H. T. Hoffman, L. H. Karnell, G. F. Funk, R. A. Robinson, H. R. J. A. o. O. H. Menck, and N. Surgery, "The National Cancer Data Base report on cancer of the head and neck," vol. 124, no. 9, pp. 951-962, 1998.

[4] W.-J. Lin, R.-S. Jiang, S.-H. Wu, F.-J. Chen, and S.-A. J. J. o. o. Liu, "Smoking, alcohol, and betel quid and oral cancer: a prospective cohort study," vol. 2011, 2011.

[5] C. R. Leemans, B. J. Braakhuis, and R. H. J. N. r. c. Brakenhoff, "The molecular biology of head and neck cancer," vol. 11, no. 1, p. 9, 2011.

[6] E. Alsahafi et al., "Clinical update on head and neck cancer: molecular biology and ongoing challenges," vol. 10, no. 8, pp. 1-17, 2019.

[7] A. Argiris, M. V. Karamouzis, D. Raben, and R. L. J. T. L. Ferris, "Head and neck cancer," vol. 371, no. 9625, pp. 1695-1709, 2008.

[8] A. Forastiere, W. Koch, A. Trotti, and D. J. N. E. J. o. M.

Sidransky, "Head and neck cancer," vol. 345, no. 26, pp. 1890-1900, 2001.

[9] R. I. Haddad and D. M. J. N. E. J. o. M. Shin, "Recent advances in head and neck cancer," vol. 359, no. 11, pp. 1143-1154, 2008.

[10] J. B. Vermorken et al., "Cisplatin, fluorouracil, and docetaxel in unresectable head and neck cancer," vol. 357, no. 17, pp. 1695-1704, 2007.

[11] I. Dagogo-Jack and A. T. Shaw, "Tumour heterogeneity and resistance to cancer therapies," Nat Rev Clin Oncol, Review Article vol. 15, pp. 81-94, 11/08/online 2017.

[12] F. Michor and K. J. C. p. r. Polyak, "The origins and implications of intratumor heterogeneity," vol. 3, no. 11, pp. 1361-1364, 2010.

[13] A. Marusyk and K. J. B. e. B. A.-R. o. C. Polyak, "Tumor heterogeneity: causes and consequences," vol. 1805, no. 1, pp. 105-117, 2010.

[14] M. Jamal-Hanjani, S. A. Quezada, J. Larkin, and C. J. C. c. r. Swanton, "Translational implications of tumor heterogeneity," vol. 21, no. 6, pp. 1258-1266, 2015.

[15] C. J. C. r. Swanton, "Intratumor heterogeneity: evolution through space and time," vol. 72, no. 19, pp. 4875-4882, 2012.

[16] L. L. Campbell and K. J. C. c. Polyak, "Breast tumor heterogeneity: cancer stem cells or clonal evolution?," vol. 6, no. 19, pp. 2332-2338, 2007.

[17] M. Jamal-Hanjani, S. A. Quezada, J. Larkin, and C. Swanton, "Translational Implications of Tumor Heterogeneity," Clin Cancer Res, vol. 21, no. 6, pp. 1258-1266, 2015.

[18] A. Marusyk, V. Almendro, and K. Polyak, "Intra-tumour heterogeneity: a looking glass for cancer?," Nat Rev Cancer, Review Article vol. 12, pp. 323-34, 04/19/online 2012.

[19] M. Kleppe and R. L. Levine, "Tumor heterogeneity confounds and illuminates: assessing the implications," Nat Med, vol. 20, no. 4, pp. 342-4, 2014.

[20] N. McGranahan and C. Swanton, "Clonal Heterogeneity and Tumor Evolution: Past, Present, and the Future," Cell, vol. 168, no. 4, pp. 613-628, Feb 9 2017.

[21] P. L. Bedard, A. R. Hansen, M. J. Ratain, and L. L. Siu, "Tumour heterogeneity in the clinic," Nature, vol. 501, no. 7467, pp. 355-364, 2013.

[22] N. Navin et al., "Tumour evolution inferred by single-cell sequencing," Nature, vol. 472, pp. 90-94, 03/13/online 2011.

[23] M. A. Jacoby, E. J. Duncavage, and M. J. Walter, "Implications of Tumor Clonal Heterogeneity in the Era of Next-Generation Sequencing," Trends Cancer, vol. 1, no. 4, pp. 231-241, 2015/12/01/ 2015.

[24] M. Gerlinger et al., "Intratumor heterogeneity and branched evolution revealed by multiregion sequencing," vol. 366, no. 10, pp. 883-892, 2012.

[25] J. Wang, Y. J. C. Song, and t. medicine, "Single cell

sequencing: a distinct new field," vol. 6, no. 1, p. 10, 2017.

[26] A. Rajput, T. Bocklage, A. Greenbaum, J.-H. Lee, and S. A. Ness, "Mutant-Allele Tumor Heterogeneity Scores Correlate With Risk of Metastases in Colon Cancer," Clin Colorectal Cancer, vol. 16, no. 3, pp. e165-e170, 2017.

[27] F. Tixier et al., "FDG PET derived quantitative heterogeneity features reflect gene expression profiles in head and neck cancer," J Nucl Med, vol. 55, p. 450, 2014.

[28] J. J. Connolly et al., "Copy number variation analysis in the context of electronic medical records and large-scale genomics consortium efforts," vol. 5, p. 51, 2014.

[29] B. Frank et al., "Copy number variant in the candidate tumor suppressor gene MTUS1 and familial breast cancer risk," vol. 28, no. 7, pp. 1442-1445, 2007.

[30] X.-C. Li, C. Liu, T. Huang, and Y. J. B. r. i. Zhong, "The occurrence of genetic alterations during the progression of breast carcinoma," vol. 2016, 2016.

[31] J. Noorbakhsh, H. Kim, S. Namburi, and J. H. J. S. r. Chuang, "Distribution-based measures of tumor heterogeneity are sensitive to mutation calling and lack strong clinical predictive power," vol. 8, no. 1, p. 11445, 2018.

[32] W. E. Corver, L. A. Koopman, J. van der Aa, M. Regensburg, G. J. Fleuren, and C. J. J. C. T. J. o. t. I. S. f. A. C. Cornelisse, "Four-color multiparameter DNA flow cytometric method to study phenotypic intratumor heterogeneity in

cervical cancer," vol. 39, no. 2, pp. 96-107, 2000.

[33] H. Zheng et al., "Single-cell analysis reveals cancer stem cell heterogeneity in hepatocellular carcinoma," vol. 68, no. 1, pp. 127-140, 2018.

[34] F. Schmidt and T. J. P. Efferth, "Tumor heterogeneity, single-cell sequencing, and drug resistance," vol. 9, no. 2, p. 33, 2016.

[35] Y. H. Chang, G. Thibault, B. Johnson, A. Margolin, and J. W. Gray, "Integrative analysis on histopathological image for identifying cellular heterogeneity," in Medical Imaging 2017: Digital Pathology, 2017, vol. 10140, p. 101400T: International Society for Optics and Photonics.

[36] A. Sharma et al., "Non-genetic intra-tumor heterogeneity is a major predictor of phenotypic heterogeneity and ongoing evolutionary dynamics in lung tumors," vol. 29, no. 8, pp. 2164-2174. e5, 2019.

[37] L. A. Cooper, J. Kong, D. A. Gutman, W. D. Dunn, M. Nalisnik, and D. J. J. L. i. Brat, "Novel genotype-phenotype associations in human cancers enabled by advanced molecular platforms and computational analysis of whole slide images," vol. 95, no. 4, p. 366, 2015.

[38] P. Lambin et al., "Radiomics: the bridge between medical imaging and personalized medicine," (in eng), Nat Rev Clin Oncol, vol. 14, no. 12, pp. 749-762, Dec 2017.

[39] S. Chicklore, V. Goh, M. Siddique, A. Roy, P. K. Marsden,

and G. J. Cook, "Quantifying tumour heterogeneity in 18F-FDG PET/CT imaging by texture analysis," (in eng), Eur J Nucl Med Mol Imaging, vol. 40, no. 1, pp. 133-40, Jan 2013.

[40] G. J. Cook et al., "Non-Small Cell Lung Cancer Treated with Erlotinib: Heterogeneity of (18)F-FDG Uptake at PET-Association with Treatment Response and Prognosis," Radiology, vol. 276, no. 3, pp. 883-93, Sep 2015.

[41] M. Hatt, F. Tixier, L. Pierce, P. E. Kinahan, C. C. Le Rest, and D. Visvikis, "Characterization of PET/CT images using texture analysis: the past, the present… any future?," Eur J Nucl Med Mol Imaging, vol. 44, no. 1, pp. 151-165, 06/06 2017.

[42] S. H. Hyun et al., "Intratumoral heterogeneity of (18)F-FDG uptake predicts survival in patients with pancreatic ductal adenocarcinoma," Eur J Nucl Med Mol Imaging, vol. 43, no. 8, pp. 1461-8, Jul 2016.

[43] M. R. Folkert et al., "Predictive modeling of outcomes following definitive chemoradiotherapy for oropharyngeal cancer based on FDG-PET image characteristics," (in eng), Phys Med Biol, vol. 62, no. 13, pp. 5327-5343, Jul 7 2017.

[44] K. Na and H. Choi, "Tumor metabolic features identified by 18F-FDG PET correlate with gene networks of immune cell microenvironment in head and neck cancer," J Nucl Med, vol. 59, no. 1, pp. 31-37, 2018.

[45] H. Choi and K. Na, "Integrative analysis of imaging and transcriptomic data of the immune landscape associated with

tumor metabolism in lung adenocarcinoma: Clinical and prognostic implications," Theranostics, vol. 8, no. 7, p. 1956, 2018.

[46] Weber, Wolfgang A.,, and biology, "Quantitative assessment of tumor metabolism using FDG-PET imaging," vol. 27, no. 7, pp. 683-687, 2000.

[47] Kubota, K., "From tumor biology to clinical PET: a review of positron emission tomography (PET) in oncology," vol. 15, no. 6, pp. 471-486, 2001.

[48] Shields, A.F., "Positron emission tomography measurement of tumor metabolism and growth: its expanding role in oncology," vol. 8, no. 3, pp. 141-150, 2006.

[49] Hoh, Carl K, "Clinical use of FDG PET," vol. 34, no. 7, pp. 737-742, 2007.

[50] Reske, Sven N., and Jörg Kotzerke. "FDG-PET for clinical use," vol. 28, no. 11, pp. 1707-1723, 2001.

[51] L. Kostakoglu, H. Agress Jr, and S. J. J. R. Goldsmith, "Clinical role of FDG PET in evaluation of cancer patients," vol. 23, no. 2, pp. 315-340, 2003.

[52] Adams, Stefan, et al., "Prospective comparison of 18 F-FDG PET with conventional imaging modalities (CT, MRI, US) in lymph node staging of head and neck cancer," vol. 25, no. 9, pp. 1255-1260, 1998.

[53] M. Benchaou et al., "The role of FDG-PET in the preoperative assessment of N-staging in head and neck

cancer," vol. 116, no. 2, pp. 332-335, 1996.

[54] B. M. Klabbers, A. A. Lammertsma, B. J. J. M. I. Slotman, and Biology, "The value of positron emission tomography for monitoring response to radiotherapy in head and neck cancer," vol. 5, no. 4, pp. 257-270, 2003.

[55] K. Kubota et al., "FDG-PET delayed imaging for the detection of head and neck cancer recurrence after radio-chemotherapy: comparison with MRI/CT," vol. 31, no. 4, pp. 590-595, 2004.

[56] E. Kresnik et al., "Evaluation of head and neck cancer with 18 F-FDG PET: a comparison with conventional methods," vol. 28, no. 7, pp. 816-821, 2001.

[57] A. Al-Ibraheem, A. Buck, B. J. Krause, K. Scheidhauer, and M. J. J. o. o. Schwaiger, "Clinical applications of FDG PET and PET/CT in head and neck cancer," vol. 2009, 2009.

[58] S. H. Moon, S. H. Hyun, and J. Y. J. K. j. o. r. Choi, "Prognostic significance of volume-based PET parameters in cancer patients," vol. 14, no. 1, pp. 1-12, 2013.

[59] B. S. Kim, K. Pak, K.-I. Yi, I. J. Kim, H.-J. Roh, and K.-S. J. E. A. o. O.-R.-L. Cho, "Prognostic value of tumoral heterogeneity and volumetric parameters as measured by F18-FDG PET/CT in sinonasal cancer," vol. 274, no. 3, pp. 1437-1443, 2017.

[60] R. Abgral et al., "Prognostic value of volumetric parameters measured by 18 F-FDG PET/CT in patients with head and

neck squamous cell carcinoma," vol. 41, no. 4, pp. 659-667, 2014.

[61] G. Castellano, L. Bonilha, L. Li, and F. J. C. r. Cendes, "Texture analysis of medical images," vol. 59, no. 12, pp. 1061-1069, 2004.

[62] S. Chicklore et al., "Quantifying tumour heterogeneity in 18 F-FDG PET/CT imaging by texture analysis," vol. 40, no. 1, pp. 133-140, 2013.

[63] F. Tixier et al., "Intratumor heterogeneity characterized by textural features on baseline 18F-FDG PET images predicts response to concomitant radiochemotherapy in esophageal cancer," vol. 52, no. 3, pp. 369-378, 2011.

[64] F. Orlhac, M. Soussan, J.-A. Maisonobe, C. A. Garcia, B. Vanderlinden, and I. Buvat, "Tumor texture analysis in 18F-FDG PET: relationships between texture parameters, histogram indices, standardized uptake values, metabolic volumes, and total lesion glycolysis," J Nucl Med, vol. 55, no. 3, pp. 414-22, 2014.

[65] R. T. Larue, G. Defraene, D. De Ruysscher, P. Lambin, and W. J. T. B. j. o. r. Van Elmpt, "Quantitative radiomics studies for tissue characterization: a review of technology and methodological procedures," vol. 90, no. 1070, p. 20160665, 2017.

[66] H. Choi and K. Na, "Pan-cancer analysis of tumor metabolic landscape associated with genomic alterations," Mol Cancer, journal article vol. 17, no. 1, p. 150, October 17 2018.

[67] G. Joshi-Tope et al., "Reactome: a knowledgebase of biological pathways," Nucleic Acids Res, vol. 33, no. suppl_1, pp. D428-D432, 2005.

[68] C. Nioche et al., "LIFEx: A Freeware for Radiomic Feature Calculation in Multimodality Imaging to Accelerate Advances in the Characterization of Tumor Heterogeneity," Cancer Res, vol. 78, no. 16, pp. 4786-4789, Aug 15 2018.

[69] S. Han, Y. J. Kim, S. Woo, C. H. Suh, and J. J. J. C. n. m. Lee, "Prognostic value of volumetric parameters of pretreatment 18F-FDG PET/CT in esophageal cancer: a systematic review and meta-analysis," vol. 43, no. 12, pp. 887-894, 2018.

[70] T. Torizuka et al., "Prognostic value of 18F-FDG PET in patients with head and neck squamous cell cancer," vol. 192, no. 4, pp. W156-W160, 2009.

[71] L. Wang, J. Bai, and P. J. N. m. c. Duan, "Prognostic value of 18F-FDG PET/CT functional parameters in patients with head and neck cancer: a meta-analysis," vol. 40, no. 4, pp. 361-369, 2019.

[72] C. Bailly et al., "Revisiting the robustness of PET-based textural features in the context of multi-centric trials," vol. 11, no. 7, p. e0159984, 2016.

[73] A. Forgacs et al., "A study on the basic criteria for selecting heterogeneity parameters of F18-FDG PET images," vol. 11, no. 10, p. e0164113, 2016.

[74] A. Mayakonda, D.-C. Lin, Y. Assenov, C. Plass, and H. P. Koeffler, "Maftools: efficient and comprehensive analysis of somatic variants in cancer," Genome Res, vol. 28, no. 11, pp. 1747-1756, 2018.

[75] S. V. Laddha, S. Ganesan, C. S. Chan, and E. J. M. c. r. White, "Mutational landscape of the essential autophagy gene BECN1 in human cancers," vol. 12, no. 4, pp. 485-490, 2014.

[76] J. Liu et al., "An Integrated TCGA Pan-Cancer Clinical Data Resource to Drive High-Quality Survival Outcome Analytics," Cell, vol. 173, no. 2, pp. 400-416, 2018.

[77] J. Choi et al., "Association of metabolic and genetic heterogeneity in head and neck squamous cell carcinoma with prognostic implications: integration of FDG PET and genomic analysis," EJNMMI RES, vol. 9, no. 1, pp. 1-11, 2019.

[78] R.-Y. Chen et al., "Associations of Tumor PD-1 Ligands, Immunohistochemical Studies, and Textural Features in 18F-FDG PET in Squamous Cell Carcinoma of the Head and Neck," Sci Rep, vol. 8, no. 1, p. 105, 2018/01/08 2018.

[79] G. D. Wilson et al., "Glucose Metabolism Gene Expression Patterns and Tumor Uptake of 18F-Fluorodeoxyglucose After Radiation Treatment," Int J Radiat Oncol Biol Phys, vol. 90, no. 3, pp. 620-627, 2014.

[80] V. S. Nair, O. Gevaert, G. Davidzon, S. K. Plevritis, and R. West, "NF-κB protein expression associates with 18F-FDG PET tumor uptake in non-small cell lung cancer: A

radiogenomics validation study to understand tumor metabolism," Lung Cancer, vol. 83, no. 2, pp. 189-196, 2014.

[81] E. K. Hong et al., "Radiogenomics correlation between MR imaging features and major genetic profiles in glioblastoma," Eur Radiol, vol. 28, no. 10, pp. 4350-4361, 2018.

[82] T. Tohma et al., "Relationship between glucose transporter, hexokinase and FDG-PET in esophageal cancer," Hepatogastroenterology, vol. 52, no. 62, pp. 486-490, 2005.

[83] K. Hamada et al., "18 F-FDG-PET of musculoskeletal tumors: a correlation with the expression of glucose transporter 1 and hexokinase II," Ann Nucl Med, vol. 22, no. 8, pp. 699-705, 2008.

[84] T. Higashi et al., "Relationship between retention index in dual-phase 18F-FDG PET, and hexokinase-II and glucose transporter-1 expression in pancreatic cancer," J Nucl Med, vol. 43, no. 2, pp. 173-180, 2002.

[85] E. A. Mroz, A. D. Tward, R. J. Hammon, Y. Ren, and J. W. Rocco, "Intra-tumor genetic heterogeneity and mortality in head and neck cancer: analysis of data from the Cancer Genome Atlas," PLoS Med, vol. 12, no. 2, p. e1001786, Feb 2015.

[86] E. A. Mroz, A. D. Tward, C. R. Pickering, J. N. Myers, R. L. Ferris, and J. W. Rocco, "High intratumor genetic heterogeneity is related to worse outcome in patients with head and neck squamous cell carcinoma," Cancer, vol. 119, no.

16, pp. 3034-42, Aug 15 2013.

[87] S. H. Moon et al., "Correlations between metabolic texture features, genetic heterogeneity, and mutation burden in patients with lung cancer," Eur J Nucl Med Mol Imaging, journal article vol. Epub, pp. 1-9, August 25 2018.

[88] E. A. Mroz and J. W. J. O. o. Rocco, "MATH, a novel measure of intratumor genetic heterogeneity, is high in poor-outcome classes of head and neck squamous cell carcinoma," vol. 49, no. 3, pp. 211-215, 2013.

[89] A. Sarker et al., "Prognostic Implications of the SUVmax of Primary Tumors and Metastatic Lymph Node Measured by 18F-FDG PET in Patients With Uterine Cervical Cancer: A Meta-analysis," Clin Nucl Med, vol. 41, no. 1, pp. 34-40, Jan 2016.

[90] H. J. Im et al., "Prediction of tumour necrosis fractions using metabolic and volumetric 18F-FDG PET/CT indices, after one course and at the completion of neoadjuvant chemotherapy, in children and young adults with osteosarcoma," (in eng), Eur J Nucl Med Mol Imaging, vol. 39, no. 1, pp. 39-49, Jan 2012.

[91] K. Pak et al., "Prognostic Value of Metabolic Tumor Volume and Total Lesion Glycolysis in Head and Neck Cancer: A Systematic Review and Meta-Analysis," J Nucl Med, vol. 55, no. 6, pp. 884-890, Apr 21 2014.

[92] R. A. Werner et al., "Volumetric and texture analysis of pretherapeutic 18F-FDG PET can predict overall survival in

medullary thyroid cancer patients treated with Vandetanib," Endocrine, journal article vol. Epub, pp. 1-8, September 11 2018.

[93] R. A. Bundschuh et al., "Textural Parameters of Tumor Heterogeneity in (1)(8)F-FDG PET/CT for Therapy Response Assessment and Prognosis in Patients with Locally Advanced Rectal Cancer," (in eng), J Nucl Med, vol. 55, no. 6, pp. 891-7, Jun 2014.

[94] J. P. O'Connor, C. J. Rose, J. C. Waterton, R. A. Carano, G. J. Parker, and A. Jackson, "Imaging intratumor heterogeneity: role in therapy response, resistance, and clinical outcome," (in eng), Clin Cancer Res, vol. 21, no. 2, pp. 249-57, Jan 15 2015.

[95] H. J. Im, Y. K. Kim, Y. I. Kim, J. J. Lee, W. W. Lee, and S. E. Kim, "Usefulness of Combined Metabolic-Volumetric Indices of (18)F-FDG PET/CT for the Early Prediction of Neoadjuvant Chemotherapy Outcomes in Breast Cancer," Nucl Med Mol Imaging, vol. 47, no. 1, pp. 36-43, Mar 2013.

[96] J. W. Lee et al., "Prognostic Value of Metabolic Tumor Volume and Total Lesion Glycolysis on Preoperative 18F-FDG PET/CT in Patients with Pancreatic Cancer," J Nucl Med, vol. 55, no. 6, pp. 898-904, Apr 7 2014.

[97] M. Hatt et al., "18F-FDG PET uptake characterization through texture analysis: investigating the complementary nature of heterogeneity and functional tumor volume in a multi-cancer site patient cohort," J Nucl Med, vol. 56, no. 1,

pp. 38-44, 2015.

[98] M. Hatt, C. Cheze-le Rest, A. Van Baardwijk, P. Lambin, O. Pradier, and D. Visvikis, "Impact of tumor size and tracer uptake heterogeneity in (18) F-FDG PET and CT non-small cell lung cancer tumor delineation," J Nucl Med, vol. 52, no. 11, pp. 1690-1697, 2011.

[99] R. A. Cairns, I. S. Harris, and T. W. Mak, "Regulation of cancer cell metabolism," Nat Rev Cancer, Review Article vol. 11, p. 85, 01/24/online 2011.

[100] D. Kumar, "Regulation of glycolysis in head and neck squamous cell carcinoma," Postdoc J, vol. 5, no. 1, pp. 14-28, Jan 2017.

[101] D. Croft et al., "The Reactome pathway knowledgebase," Nucleic Acids Res, vol. 42, no. Database issue, pp. D472-7, Jan 2014.

[102] U. Haberkorn et al., "FDG uptake, tumor proliferation and expression of glycolysis associated genes in animal tumor models," Nucl Med Biol, vol. 21, no. 6, pp. 827-834, 1994/08/01/ 1994.

[103] H. Schoder, Y. E. Erdi, K. Chao, and M. Gonen, "Clinical implications of different image reconstruction parameters for interpretation of whole-body PET studies in cancer patients," J Nucl Med, vol. 45, no. 4, pp. 559-66, 2004.

국문초록

두경부 편평세포암종에서의 종양 대사 및 이질성에 대한 라디오지노믹스 분석: FDG PET 및 유전체의 통합적 분석

최진영
방사선융합의생명전공, 융합과학부
융합과학기술대학원
서울대학교

종양의 이질성에 대한 대사적 특성과 유전적 특성의 상관관계는 잘 연구되지 않았다. 이 연구는 FDG PET과 유전체 데이터로부터 얻어진 각각의 종양 이질성 특징의 관련성을 평가하고, 서로 다른 두 특징을 조합하여 잠재적인 예후 예측 인자를 평가하고자 하였다.

유전적, 임상 및 FDG PET 데이터는 the cancer genome atlas (TCGA)와 the cancer imaging archive (TCIA)의 머리 및 목 편평세포암종 데이터셋에서 얻어졌다. 유전적 종양 이질성 특성인 The mutant-allele tumor heterogeneity (MATH) score (n=508)와 종양 해당작용 특성 (GlycoS, n= 503) 이 유전체 데이터로부터 얻어졌다. 33명의 환자에서 FDG PET 데이터를 얻었다. 그 결과, 2가지의 종양 대사 특성 (SUVmax, SUVpeak), 두 개의 종양 대사-부피 특성 (MTV, TLG), 두 가지의 종양 대사적 이질성 특성 [entropy, coefficient of variation

(COV)]이 원발성 종양에서 얻어졌다.

25명의 환자가 MATH와 FDG PET 데이터가 함께 분석되었다. FDG PET 특성 중에서, MTV (P = .01), TLG (P = .02), entropy (P = .01), COV (P = .04) 가 MATH와 통계적으로 유의한 상관관계를 보였다. 우리는 적은 환자 수 때문에 GlycoS를 대사적 영상 특성 대신에 생존분석에 사용하였다. 499명의 환자에서 MATH와 GlycoS 특성이 얻어졌다. 또한, 높은 MATH와 GlycoS는 의미가 있게 낮은 전체 생존율과 관련 있었다. (n = 499, P = 0.002 and 0.0001 for MATH and GlycoS, respectively). 뿐만 아니라, MATH와 GlycoS는 임상 병리학적 특성을 포함하여 조정된 모델에서도 전체 생존에 대한 예후를 예측할 수 있었다. (P = 0.015 and 0.006, respectively).

머리 및 목 편평세포암종 환자에서 FDG PET에 의해 평가된 종양 이질성 파라미터는 유전체 데이터에 의해 얻어진 종양 이질성 특성과 관련이 있었다. 해당작용과 유전체 데이터에 의해 얻어진 종양 이질성 특성은 환자의 예후를 더욱 계층화 할 수 있으며, 이는 정확한 예후를 위해 유전체 및 대사적 특징을 모두 사용할 가능성을 이야기한다.

……

주요어 : ^{18}F-플루오로데옥시글루코스, 양전자 방사 단층 촬영, 이질성, 방사선유전학, MATH

학 번 : 2018-29025